HM Hochschule für angewandte Wissenschaften München
Alexander Edelemann, supervised by Prof. Gramich

Praktikum Nanotechnik
January 22, 2025

Photoluminescence of Semiconductor Heterostructure Quantum Wells

CONTENTS

1 THE MULTI-LAYER HETEROSTRUCTURE

Modern epitaxy techniques for semiconductor layers, such as molecular beam epitaxy (MBE) and metal-organic vapor phase epitaxy (MOVPE), enable the precise deposition of two different semiconductors with distinct band gaps on top of each other. These layer structures are crucial for modern applications, particularly in components made from III-V semiconductors like GaAs and InP. These epitaxy processes can also produce ternary or quaternary alloys, such as $Al_xGa_{1-x}As$, whose band gaps lie between those of their corresponding binary compounds. By selectively varying the composition x in $Al_xGa_{1-x}As$, the electronic band structure can be continuously tuned between that of GaAs and AlAs. Notably, at $x = 0.45$, the alloy transitions from a direct to an indirect semiconductor. This flexibility is particularly advantageous because semiconductors with closely matched lattice constants grow epitaxially with minimal defects. For instance, Ge can be epitaxially grown on GaAs, and vice versa, achieving excellent lattice matching. Similarly, the GaAlAs alloy system offers band gap tunability between approximately 1.4 eV and 2.2 eV, with excellent crystalline quality due to the near-perfect lattice matching of GaAs and AlAs. When two different semiconductors are grown epitaxially on top of each other, the resulting structure is called a semiconductor heterostructure. Advanced epitaxy techniques allow for transitions between materials to be sharp, often within the range of a single atomic layer. Consequently, the band gap in such heterostructures can vary over atomic dimensions, providing exceptional control over electronic and optical properties. This enables the fabrication of quantum wells restricting electrons and holes alike to discrete energy states for instance by enclosing a thin GaAs layer between two $Al_xGa_{1-x}As$ compounds. In such a system electrons form a 2-dimensional gas of electron whose energy in lateral direction is restricted to discrete levels. These energy bands of electrons confined in two dimensions are known as subbands and are described by vertically separated parabolas

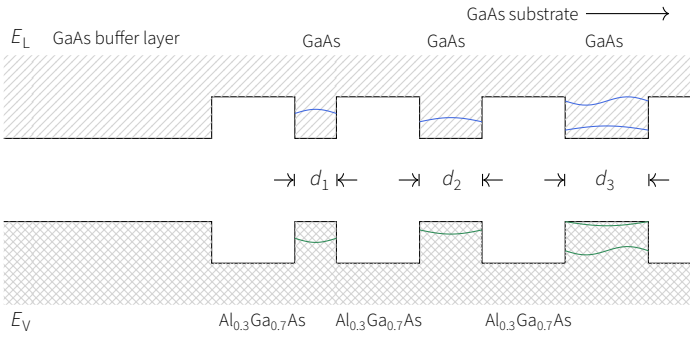

Fig. 1 | Schematic illustration of the multilayer heterostructure used in this experiment. The GaAs potential wells of width d are each separated by an $Al_{0.3}Ga_{0.7}As$ barrier of width 300 Å. Sufficiently shrinking the width of the $Al_{0.3}Ga_{0.7}As$ barrier will result in a splitting of the discrete energy states into bands.

in k-space. The existence of these quantum wells can be verified by means of photoluminescence experiments [1, 2].

In this study, we investigate a multilayer heterostructure epitaxially grown on a GaAs substrate consisting of multiple GaAs quantum wells of varying width d each separated from the others by a 300 Å thick $Al_{0.3}Ga_{0.7}As$ barrier, as schematically illustrated in Fig. 1. The six different widths of these wells a listed in Tab. 1. The sample was mounted in a variable temperature cryostat to measure its excitation photoluminescence spectrum across different temperatures.

GaAs-layer	thickness [Å]
d_1	20
d_2	30
d_3	50
d_4	70
d_5	100
d_5	200

Tab. 1 | Thicknesses d of the GaAs-layers within the sample in which quantum confinement occurs.

2 IDENTIFICATION OF EMISSION PEAKS

As the cryostat's temperature was gradually lowered, photoluminescence spectra were recorded across different temperature

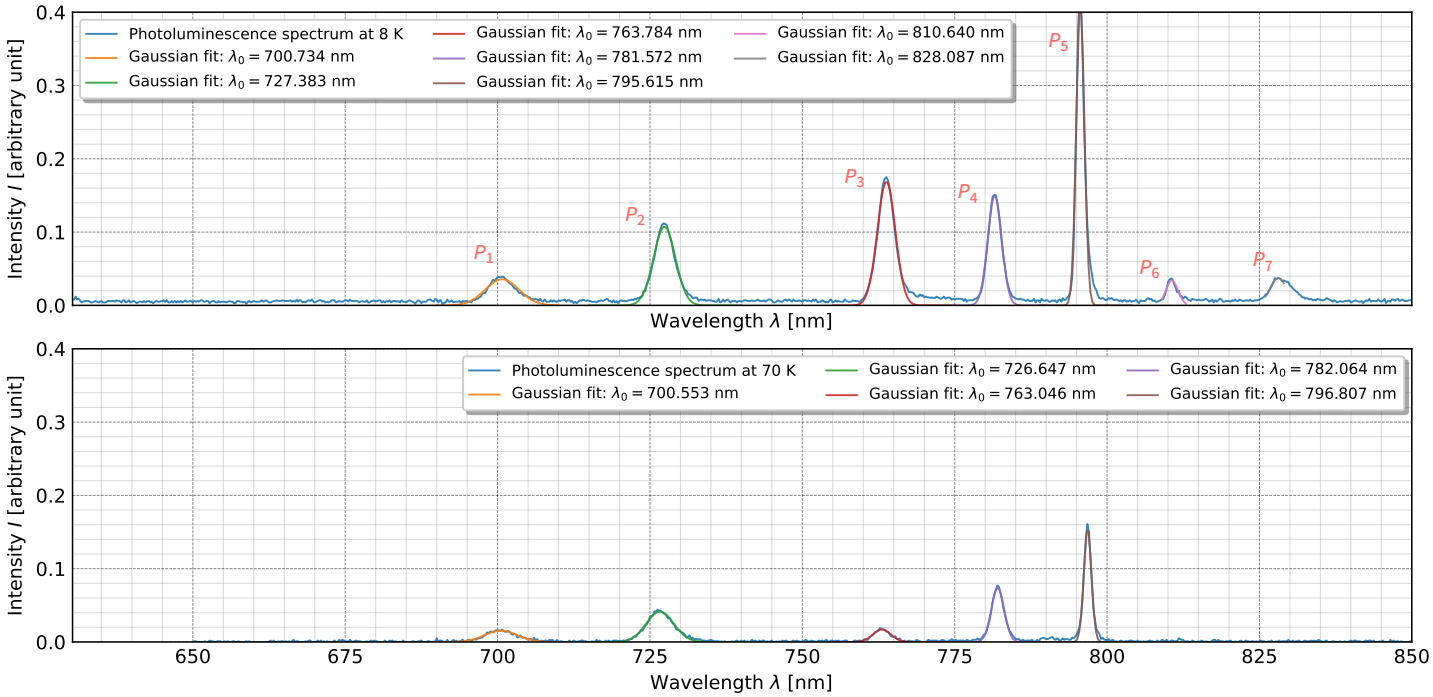

Fig. 2 | Photoluminescence spectra. *Top*: Spectrum recorded a constant temperature T = 8 K. *Bottom*: Spectrum recorded a constant temperature T = 70 K.

ranges. At higher temperatures, the spectrum is dominated by the peak corresponding to the laser used for excitation. The laser, specified to have a center wavelength of 634 nm, was observed at approximately 632 nm in the recorded data, indicating a calibration error of about 2 nm in the measurement system. As the temperature decreases, the photoluminescence peaks of the sample become more pronounced, revealing the sample's optical transitions with greater clarity. High-resolution spectra were captured at constant temperatures of 8 K (the lowest achievable temperature) and 70 K, as shown in Fig. 2. In the spectrum recorded at 8 K, additional peaks are observed, likely due to the suppression of phonon-assisted transitions at lower temperatures. We fit each observed photoluminescence peak at 8 K and 70 K to a Gaussian function to extract its center wavelength. The center wavelengths, subtracted by 2 nm to account for the calibration offset, for all observed peaks at 8 K are summarized in Table 2.

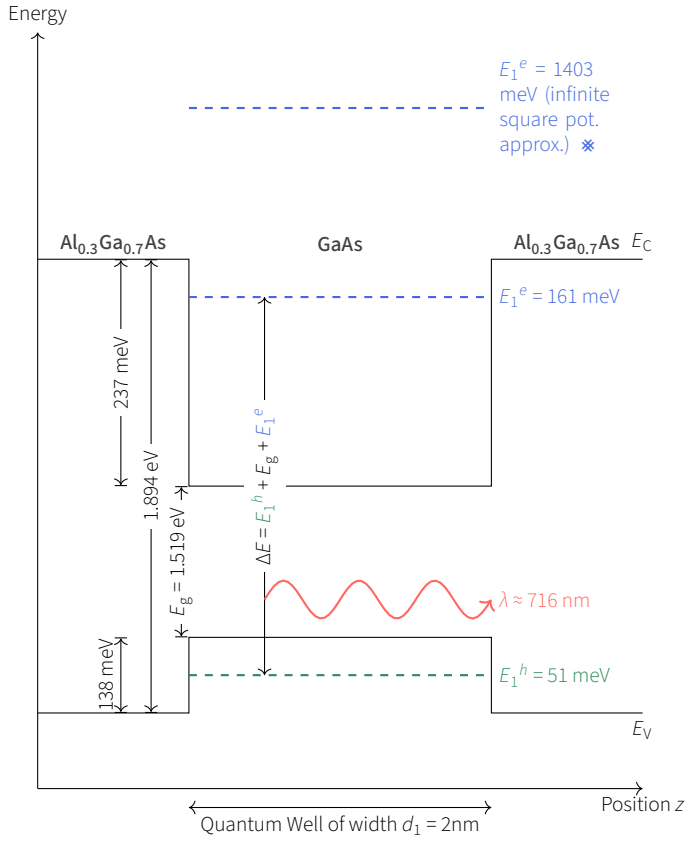

Fig. 3 | Schematic illustration of the energy band structure for a GaAs $Al_{0.3}Ga_{0.7}As$ quantum well of width d = 2 nm. (Drawing not to scale.)

peak	wavelength [nm]	Energy [eV]	E - E_G [eV]
P_1	698.734	1.774	0.255
P_2	725.383	1.709	0.190
P_3	761.784	1.628	0.104
P_4	779.572	1.590	0.071
P_5	793.615	1.562	0.043
P_6	808.640	1.533	0.014
P_7	826.087	1.501	-0.018※

Tab. 2 | Data extracted from the photoluminescence spectrum recorded at 8 K by fitting a Gaussian to each observed peak.

Identifying the individual peaks requires a detailed understanding of the $Al_{0.3}Ga_{0.7}As$/GaAs heterostructure's band structure. For the GaAs layer with a thickness of $d_1 = 2$ nm, this band structure is illustrated in Fig. 3. The conduction and valence bands of GaAs form quantum wells due to the band offsets relative to the surrounding AlGaAs layers: the conduction band of GaAs lies below that of AlGaAs, while the valence band lies above. These quantum wells confine electrons and holes, resulting in discrete energy states (subbands) within the wells. The spacing of these subbands depends on the well width. Optical transitions can occur between the n-th conduction subband (marked in blue) and the n-th valence subband (marked in green). Consequently, photoluminescence measurements capture the energy differences between

these subbands, corresponding to intersubband transitions, rather than the absolute energies of individual subbands.

Band gap The identification of the transitions observed in the recorded data requires the knowledge of the size of the band gap of GaAs. This value is temperature dependent and at 0 K it is $E_g(0) = 1.519\,\text{eV}$. The band gap energy increases as the temperature decreases. This trend is evident in the recorded data, where peaks at higher wavelengths shift slightly toward lower wavelengths with decreasing temperature. For semiconductors such as GaAs, the temperature dependence of the band gap $E_g(T)$ can be described by the empirical Varshni equation:

$$E_g(T) = E_g(0) - \frac{\alpha T^2}{T + \beta},$$

where α is a material-dependent coefficient that quantifies the rate of change of the band gap with temperature, and β is related to the material's Debye temperature. For GaAs, the typical parameters are:

$$\alpha \approx 5.405 \times 10^{-4}\,\text{eV/K}, \quad \beta \approx 204\,\text{K}.$$

Especially for intermediate and higher temperatures, it is essential to account for this temperature-dependence. In our case however, our recorded data (at 8 K) is sufficiently close to absolute zero temperature that this effect is negligible. Hence, we use $E_g(8\,\text{K}) \approx 1.519\,\text{eV}$.

Energy subbands The individual energy levels of electrons and holes within the quantum wells can be determined by solving the Schrödinger equation for a square well potential defined as:

$$V(z) = \begin{cases} 0, & \text{for } 0 < z < d, \\ V_0, & \text{for } z \geq d \text{ or } z \leq 0, \end{cases}$$

where V_0 represents the band offsets of GaAs relative to the surrounding AlGaAs. The solutions to this equation yield energy levels with even and odd parity, determined by the following transcendental conditions:

$$\tan\left(\frac{kd}{2}\right) = \frac{m_T^* \kappa}{m_B^* k}, \quad \text{(even parity)},$$

$$\cot\left(\frac{kd}{2}\right) = -\frac{m_T^* \kappa}{m_B^* k}, \quad \text{(odd parity)}.$$

Here, m_T^* and m_B^* represent the effective masses of carriers in the quantum well and barrier, respectively. The parameters k and κ are given by:

$$k = \frac{1}{\hbar}\sqrt{2m_T^* E_i}, \quad \kappa = \frac{1}{\hbar}\sqrt{2m_B^*(V_0 - E_i)},$$

where E_i is the energy level of the electrons and holes respectively. The detailed derivation of these expressions, which is both intricate and lengthy, can be found in [3]. Utilizing the semiconductor material data provided in [4], the final solutions for the first two electron subbands have been computed and are plotted in Fig. 4.

Utilizing the numerically computed energy states corresponding to different well widths the energy of the potoluminescence peaks can be separated:

$$E_p^n = E_i^e + E_i^h + E_g$$

Using the above equation, possible transitions that best fit our potoluminescence peaks are summarized in Tab. 3. It is evident from the table that the deviation between the measured peak energies and the theoretically expected values is more pronounced

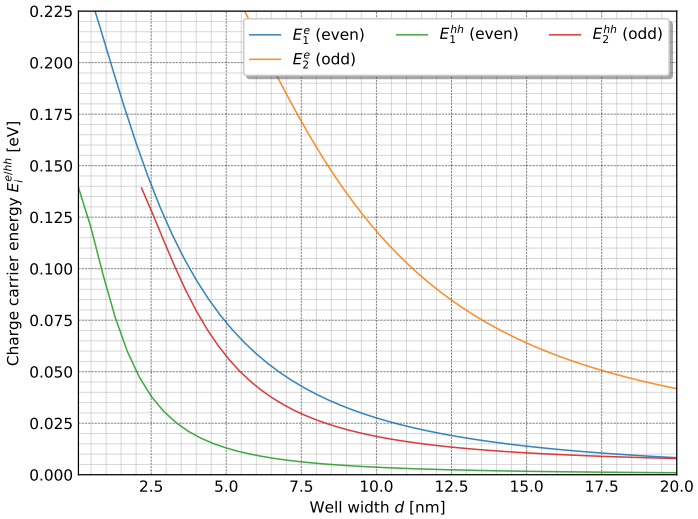

Fig. 4 | Numerical solution of the Schrödinger equation of square potential quantum wells with barrier height V_0 and width d defined by the GaAs $Al_{0.3}Ga_{0.7}As$ sandwich structure. *Blue and orange*: First two subbands for allowed electron states. *Green and red*: First two subbands for allowed heavy hole states.

at shorter wavelengths (higher energies). This occurs because the energy becomes increasingly sensitive to small changes in wavelength as the wavelength decreases:

$$\frac{\mathrm{d}E}{\mathrm{d}\lambda} \propto \frac{1}{\lambda^2}$$

Therefore, in our spectrum the higher-energy peaks appear less localized as the data is plotted with respect to wavelength and not frequency. Our spectrum was recorded at constant wavelength intervals, hence the number of data points for a constant energy interval decreases with higher energies, which also contributes to greater deviations from the theoretical values.

peak	layer-thickness [Å]	transition	Measured Energy [eV]	Theoretical Energy [eV]
P_1	20	$E_1{}^e \rightarrow E_1{}^h$	1.774	1.731
P_2	30	$E_1{}^e \rightarrow E_1{}^h$	1.709	1.672
P_3	50	$E_1{}^e \rightarrow E_1{}^h$	1.628	1.610
P_4	70	$E_1{}^e \rightarrow E_1{}^h$	1.590	1.577
P_5	100	$E_1{}^e \rightarrow E_1{}^h$	1.562	1.554
P_6	200	$E_1{}^e \rightarrow E_1{}^h$	1.533	1.530
P_7	GaAs-substrate	$E_C \rightarrow E_V$	1.501	1.519

Tab. 3 | Identification of electron transitions observed in the photoluminescence spectrum recorded at 8 K (Fig. 2, top).

Infinite barrier height approximation In certain scenarios, potential wells can be simplified by assuming infinitely high barrier heights, which makes solving the Schrödinger equation analytically feasible. This approximation provides solutions for energy levels as:

$$E_n = \frac{\hbar^2}{2m^*}\left(\frac{n\pi}{d}\right)^2,$$

where m^* is the effective mass of either electrons or holes, n is the quantum number, and d denotes the well width. The computed energy values for the first subband ($n = 1$) using this approximation are presented in Table 4.

When comparing these values with the results depicted in Fig. 4 (blue line), it becomes apparent that for wider wells, the infinite barrier height approximation can be a valid representation,

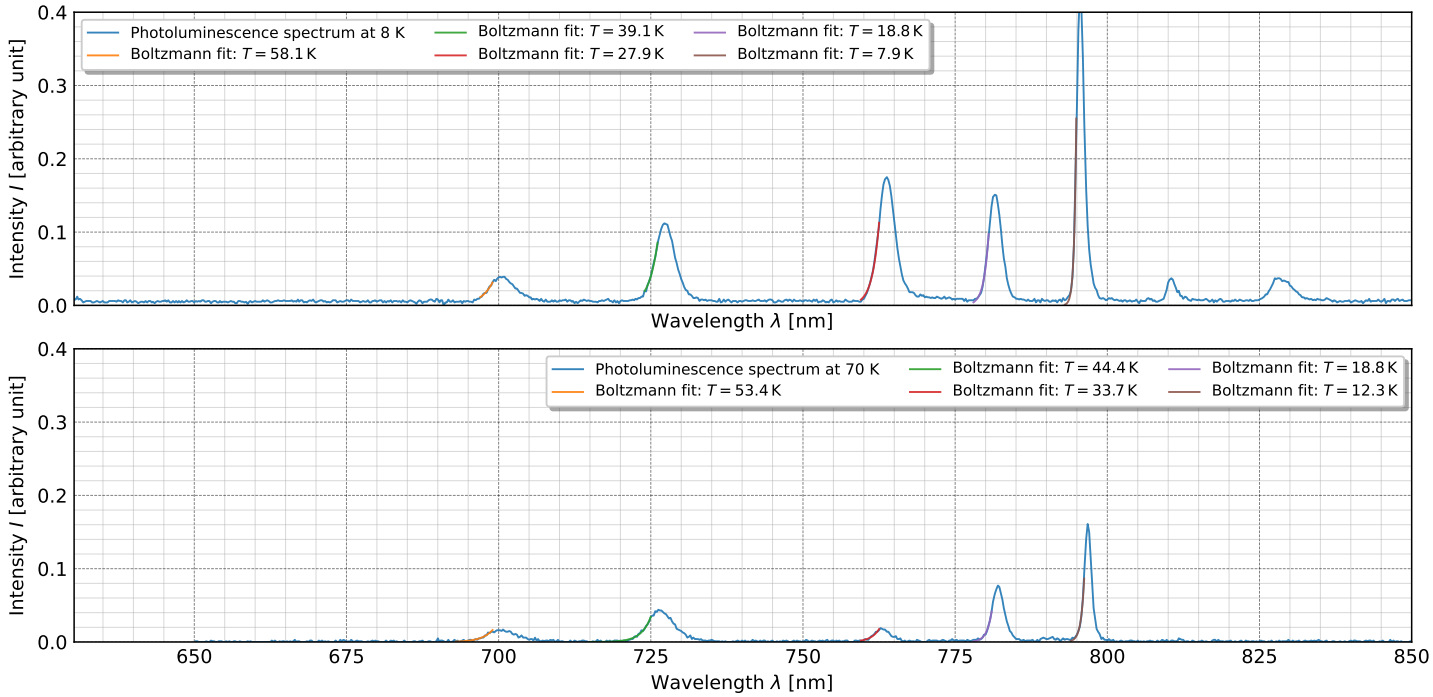

Fig. 5 | Determination of charge carrier temperature by fitting a Boltzmann distribution to the high energy tail of sufficiently pronounced peaks.

depending on the desired accuracy of the application. However, notable deviations are observed for narrower wells. In such instances, the analytical solutions may predict energy states positioned above the actual barrier height, which is not physically possible. This discrepancy underscores the limitations of the infinite barrier approximation, particularly for small well widths where the finite potential barrier height plays a crucial role.

thickness d	Energy E_1
d_1 = 20 Å	1.403 eV
d_1 = 30 Å	0.624 eV
d_1 = 50 Å	0.224 eV
d_1 = 70 Å	0.115 eV
d_1 = 100 Å	0.056 eV
d_1 = 200 Å	0.014 eV

Tab. 4 | Allowed electron states for quantum wells of varying width d with infinitely high potential barriers V_0.

3 ESTIMATION OF CHARGE CARRIER TEMPERATURE

The intensity and spectral shape of photoluminescence are highly sensitive to the thermal distribution of charge carriers (electrons and holes) within the material. In the non-degenerate regime, the photoluminescence emission can often be described using a distribution function, such as the Maxwell-Boltzmann distribution. By analyzing the high-energy tail of the photoluminescence spectrum, which is particularly temperature-sensitive, the carrier temperature can be extracted. The photoluminescence intensity $I(E)$ of the individual peaks for energies $E > E_g$ can be modeled as:

$$I(E) \propto \sqrt{E - E_g} \exp\left(-\frac{E - E_g}{k_B T}\right),$$

where E_g is the size of the energy transition, k_B is the Boltzmann constant, and T is the carrier temperature. Fitting the high-energy tail of the photoluminescence spectrum to this theoretical model provides a direct method to determine the carrier temperature. Notably, the carrier temperature can deviate from the lattice temperature due to non-equilibrium conditions induced by optical excitation. Under high-intensity excitation, electron-electron and hole-hole interactions can dominate over carrier-phonon interactions. In such cases, electrons and holes can achieve a temperature significantly higher than the lattice temperature [5].

In our analysis, we extracted the carrier temperature at 8 K and 70 K by fitting the high-energy tail of each sufficiently pronounced photoluminescence peak to the exponential term $\exp\left[-(E - E_g)(k_B T)\right]$. The center wavelengths obtained from Gaussian fits were used to calculate the corresponding E_g for each peak. The results of these fits are presented in Fig. 5. The temperature values obtained from our fits exhibit significant variance, indicating that they can only be considered rough approximations. This large variance is likely due to an insufficient number of measurement data points, making precise fitting challenging. To achieve a more accurate determination of the charge carrier temperature, more detailed and higher-resolution data is required. However, despite the limitations, a notable trend is observed: the carrier temperature appears to increase with increasing peak energy. This trend suggests a potential correlation that warrants further investigation with improved measurement precision.

REFERENCES

[1] Harald Ibach and Hans Lüth. “Semiconductors”. In: *Solid-State Physics: An Introduction to Principles of Materials Science*. Berlin, Heidelberg: Springer Berlin Heidelberg, 2009, pp. 419–515.

[2] Peter Y. Yu and Manuel Cardona. “Effect of Quantum Confinement on Electrons and Phonons in Semiconductors”. In: *Fundamentals of Semiconductors: Physics and Materials Properties*. Berlin, Heidelberg:

Springer Berlin Heidelberg, 2010, pp. 469–551. ISBN: 978-3-642-00710-1. DOI: 10.1007/978-3-642-00710-1_9. URL: https://doi.org/10.1007/978-3-642-00710-1_9.

[3] E.L. Ivchenko and G. Pikus. *Superlattices and Other Heterostructures: Symmetry and Optical Phenomena*. Springer Series in Solid-State Sciences. Springer Berlin Heidelberg, 2012. ISBN: 9783642606502. URL: https://books.google.de/books?id=Q-70CAAAQBAJ.

[4] Adachi. *$Al_xGa_{1-x}As$ – Band structure and carrier concentration*. Ioffe Institute. URL: http://www.ioffe.ru/SVA/NSM/Semicond/AlGaAs/bandstr.html.

[5] Peter Y. Yu and Manuel Cardona. "Optical Properties II". In: *Fundamentals of Semiconductors: Physics and Materials Properties*. Berlin, Heidelberg: Springer Berlin Heidelberg, 2010, pp. 345–426. ISBN: 978-3-642-00710-1. DOI: 10.1007/978-3-642-00710-1_9. URL: https://doi.org/10.1007/978-3-642-00710-1_9.